Article

Tuning of NASA Standard Breakup Model for Fragmentation Events Modelling

Nicola Cimmino [1,*], **Giorgio Isoletta** [1], **Roberto Opromolla** [1], **Giancarmine Fasano** [1], **Aniello Basile** [2], **Antonio Romano** [2], **Moreno Peroni** [3], **Alessandro Panico** [3] and **Andrea Cecchini** [3]

[1] Department of Industrial Engineering, University of Naples "Federico II", P.le Tecchio 80, 80125 Naples, Italy; giorgio.isoletta@unina.it (G.I.); roberto.opromolla@unina.it (R.O.); giancarmine.fasano@unina.it (G.F.)

[2] Vitrociset S.p.A., 00156 Rome, Italy; a.basile.somm@vitrociset.it (A.B.); a.romano@vitrociset.it (A.R.)

[3] Flight Test Wing of the Italian Air Force, 00040 Pomezia, Italy; moreno.peroni@aeronautica.difesa.it (M.P.); alessandro1.panico@aeronautica.difesa.it (A.P.); andrea1.cecchini@aeronautica.difesa.it (A.C.)

* Correspondence: nicola.cimmino@unina.it

Abstract: The continuous growth of space debris motivates the development and the improvement of tools that support the monitoring of a more and more congested space environment. Satellite breakup models play a key role to predict and analyze orbital debris evolution, and the NASA Standard Breakup Model represents a widely used reference, with current activities relevant to its evolution and improvements especially towards fragmentation of small mass spacecraft. From an operational perspective, an important point for fragmentation modelling concerns the tuning of the breakup model to achieve consistency with orbital data of observed fragments. In this framework, this paper proposes an iterative approach to estimate the model inputs, and in particular, the parents' masses involved in a collision event. The iterative logic exploits the knowledge of Two Line Elements (TLE) of the fragments at some time after the event to adjust the input parameters of the breakup model with the objective of obtaining the same number of real fragments within a certain tolerance. Atmospheric re-entry is accounted for. As a result, the breakup model outputs a set of fragments whose statistical distribution, in terms of number and size, is consistent with the catalogued ones. The iterative approach is demonstrated for two different scenarios (i.e., catastrophic collision and non-catastrophic collision) using numerical simulations. Then, it is also applied to a real collision event.

Keywords: space debris; space surveillance and tracking; fragmentation events modelling; NASA standard breakup model; collision modelling

1. Introduction

Space debris is a threat to the safe operation of satellites and the long-term sustainability of space activities. The generation of space debris via collisions and explosions in orbit could lead to an exponential increase in the number of artificial objects in space in a chain reaction known as Kessler Syndrome [1]. Nowadays, among the more than 8700 objects larger than 10 cm in Earth orbits, only about 6% are operational satellites, whereas the remainder is space debris. In addition, there are many smaller objects that are not routinely tracked, with estimates for the number of objects larger than 1 cm ranging from 100,000 to 200,000 [2] and an estimated 128 million particles between 1 mm and 1 cm [3]. Fragments of 1 cm size are particularly critical since they are very hard to detect, even in lower orbits, but can be mission-ending for operating satellites due to their high speed and, consequently, associated impact energy.

The dominant source of space debris by number of objects are breakup events, mainly due to on-orbit explosions and collisions. There are several reasons for breakup events, labelled by ESA Database and Information System Characterising Objects in Space (DIS-COS) as follows [4]: (i) propulsion: stored energy for non-passivated propulsion-related subsystems might lead to an explosion, for example due to thermal stress; (ii) upper stages

explosions due to residual propellants; (iii) ullage motors; (iv) electrical: overcharging and subsequent explosion of batteries; (v) aerodynamics: breakup most often caused by an overpressure due to atmospheric drag; (vi) collision between two objects called *parents*, usually referred to as *target* (i.e., the primary or larger object) and *projectile* (i.e., the secondary or smaller object); (vii) deliberate: intentional breakup events; (viii) anti-satellite tests (ASAT); (ix) anomalous: defined as "the unplanned separation, usually at low velocity, of one or more detectable objects from a satellite that remains essentially intact".

Some of the events result in only a few objects, which might even quickly decay due to the atmospheric drag. In all the other cases, a large quantity of fragments is generated, thus significantly contributing to the increase in the collision risk that satellites are facing during their operational life [4]. While implementing debris mitigation policies, space agencies and academia continuously develop models and software to analyze the space environment, estimating the collision probability between catalogued space objects and predicting future growth of debris population [2–11].

A fundamental component of any orbital debris environment evolution model is the satellite breakup model. The worldwide reference is the NASA Standard Breakup Model (SBM) implemented both in EVOLVE 4.0 [12] and later in LEGEND [9]. It provides three fundamental outputs: fragment size, area-to-mass ratio (A/M), and relative velocity (ΔV) distributions [13]. Such distributions were obtained by a broad variety of data coming from deliberate hypervelocity collisions in Low Earth Orbit (LEO), ground-based impacts, and upper stage explosion tests, as well as from an extensive compilation of historical orbital data (i.e., TLE sets) for debris generated by explosions and collisions [12].

Due to the semiempirical and statistical nature of the SBM, there are two major research paths concerning breakup models. On the one hand, there is the need to continuously update the list of catalogued space objects to have better data fitting. For this reason, a major effort made by different players in the space industry was to track and image space objects down to 1 cm at altitudes up to 1000 km, and down to 2 mm at low LEO altitudes [2] thanks to the development of high performance ground-based RADAR systems (e.g., Space Fence, Haystack, TIRA, LeoLabs) [14–16]. Moreover, other works aim to improve collision modelling via tests on new generation satellites, as a clear trend can be seen towards smaller and lower mass spacecraft [17]. Simulations on Cosmos 2251-Iridium 33 collision and Fengyun-1C ASAT test demonstrated that while Cosmos 2251 fragments are well-described by the NASA SBM, noticeable discrepancies exist between the model predictions and the observation data for the Iridium 33 satellite and Fengyun-1C ASAT. The justification is that Cosmos 2251 was an older satellite while Iridium 33 and the Fengyun-1C weather satellites were relatively modern [13,18,19]. Hence, NASA DebriSat project aims to characterize fragments generated by hypervelocity collisions involving a modern satellite in LEO. There are three phases to this project: the design and fabrication of DebriSat—an engineering model representing a modern, 60 cm/50 kg class LEO satellite; conduction of a laboratory-based hypervelocity impact to catastrophically break up the satellite, and characterization of the properties of breakup fragments down to 2 mm in size [13,18,19]. Similarly, other experiments were carried out to characterize micro-satellite impacts (20 cm/1.5 kg), both at hyper and low velocity, varying impact directions and investigating fragments from multilayer insulation and solar cells [20,21]. Such experiments demonstrated that, although the SBM well represents the size distribution, mass and A/M distributions are greatly influenced by the materials adopted [20,21].

Other software programs like IMPACT [22,23] introduce other inputs in the breakup model to better characterize the physical properties distribution of the fragments: the type of object (i.e., hollow or compact), the material density or, in case of explosion, the amount of energy driving the explosion (e.g., chemical energy, pressure, electrical energy). Moreover, while in the SBM the standard condition for a complete fragmentation is that the kinetic energy of the projectile relative to the target divided by the target mass is greater than 40 J/g, IMPACT introduces a further value of 10 J/g to smooth the transition from

a typical hypervelocity collision with large numbers of small fragments to lower energy collisions where most of the target object is broken into a few larger fragments [24].

The second research area regards the estimation of the input data of the SBM to model real fragmentation events. In the case of collisions, the input data are the mass of the two colliding objects, M_1 and M_2, and the impact velocity v_{imp} (i.e., the norm of the relative velocity). In the case of explosions, instead, an important role is played by the scale factor of the SBM, assuming a default value of 1 for upper stages with mass between 600 kg and 1000 kg [12]. Several works [4,25–27], however, demonstrated that, giving such inputs, the number and the characteristics of the simulated fragments are different to the ones generated by a real breakup event. In particular, Anz–Meador and Matney [25] and Braun et al. [4] demonstrated that several debris clouds derived from explosions of nominal upper stages are represented by values of the scale factor significantly different from 1. Similarly, Pardini and Anselmo [27] show that out of four on-orbit accidental collisions, all having an energy-to-mass ratio greater than 40 J/g, only one generated a number of fragments similar to the one predicted by the SBM. The reason is that the breakup model is purely energy-based and does not consider the relative attitude between the two colliding objects nor the point of collision. Indeed, the basic implementation of the SBM assumes that collisions will always involve the entire body of each parent. This does not account for spacecraft consisting of multiple connected structures; for instance, the presence of appendages such as gravity gradient booms or deployed solar panels. In this respect, the effect of a collision is clearly different if the projectile hits the main body of a satellite or only a part of it. In the latter case, the fragmented mass of the two objects will be probably lower and the breakup model would overestimate the number of the debris produced. Similarly, for explosions, the uncertainty regards the energy driving the breakup and, hence, the actual exploded mass. Therefore, a good estimation of the fragmented masses of the parents is critical to correctly set the input parameters of the SBM.

For the estimation of the scale factor, a simple procedure can be adopted as in [28]: assuming that a certain number of fragments (N^*) over a minimum trackable size was catalogued, the scale factor can be derived explicitly from the equation of the cumulative distribution of the number of fragments with respect to the characteristic length. Another approach proposed by [4] can be applied to both explosion and collision events. It consists of a dynamic scaling approach using a reported number of observed fragments (or number of catalogued fragments) multiplied by an altitude dependent catalogue incompleteness factor (so-called Henize factor) to scale the power law distribution. This procedure is used by [4] to estimate the scale factor for explosions and the total fragmented mass of the parents for collisions. The Henize factor however presents a strong discontinuity for L_c equal to 6 cm.

In this framework, this paper proposes an alternative way to estimate the tuning parameters for the SBM, focusing on the fragmented mass of the parents in case of collisions. The method requires TLE sets from the event to be analyzed. It assumes that enough time from the fragmentation event passed to have all the fragments over a certain size threshold catalogued. Moreover, decayed fragments are estimated. Hence, the breakup model is iterated until the number of simulated fragments over a predefined threshold of the characteristic length is equal to the number of real fragments, within a certain tolerance. The iteration is performed on the masses of the two parents separately after identifying the debris clouds derived from the target and the projectile. Finally, the fragmented masses of the parents are estimated using the bisection method.

An important assumption in this paper is that the parents and their orbits are known. However, a correct parent identification is not always guaranteed, thus leading to erroneously assigned objects. Several works proposed methods to identify the epoch of a fragmentation as well as the known objects involved. In particular, Frey et al. [29,30] propose a method to detect past fragmentations exploiting the convergence of mean Keplerian elements when propagating backwards in time. Tetrault et al. [31] developed a tool that determines the objects involved in the fragmentation event using back propagation and

particle distribution techniques. Dimare et al. [32], instead, define a similarity function between the orbital elements of the objects under examination to establish a metric for the identification of the fragmentation. The parent objects are found by locating the minimum of the similarity function among the various objects. Romano et al. [33] use backward propagation, pruning, and clustering algorithms to identify possible orbital intersection windows that make close encounters between objects possible. To consider erroneous assignment of the fragments to the parents, an analysis of the method performance under this circumstance is also carried out.

The remaining of the paper is organized as follows. Section 2 provides a review of the Standard Breakup Model. Section 3 describes the architecture of the SBM as implemented in this paper, focusing on the iterative approach. Section 4 shows the test cases and the results obtained. Section 5 draws some conclusions on the work presented and proposes future works.

2. Review of the Standard Breakup Model

The SBM models the fragment size, *A/M*, and ΔV distributions characterizing the debris generated by a fragmentation event [13]. In this section, a synthetic description of the SBM, as implemented in EVOLVE 4.0, is reported. For more details regarding the derivation of the equations and the coefficients used in the statistical distributions, interested readers can refer to [12].

The SBM identifies two types of fragmentation events: collisions and explosions. In case of collisions, the input data are the masses of the parents (i.e., the two colliding space objects) and the impact velocity. According to the model, collisions can be either *catastrophic* if the entire masses of the two objects are fully fragmented or *non-catastrophic* in case of fragmentation of the projectile and cratering of the target. The distinction between *catastrophic* and *non-catastrophic* collisions can be done by evaluating the relative kinetic energy of the projectile divided by the mass of the target, as shown below.

$$E_p = \frac{1}{2} \frac{m_{proj}[\text{kg}] \left(v_{imp}[\text{m/s}] \right)^2}{m_{targ}[\text{g}]} \tag{1}$$

where m_{targ} and m_{proj} are the masses of the target and projectile, respectively, while v_{imp} is the impact velocity. Specifically, the collision is defined as *catastrophic* if the value of E_p is greater than 40 J/g. In the case of *non-catastrophic* collisions, i.e., E_p is less than 40 J/g, the fragmented mass of the parents is computed as follows [12],

$$m_1 = m_{proj} \left(\frac{v_{imp}[\text{km/s}]}{1[\text{km/s}]} \right)^2 \tag{2}$$

$$m_2 = m_{targ} \left(\frac{v_{imp}[\text{km/s}]}{1[\text{km/s}]} \right)^2 \tag{3}$$

where m_1 and m_2 are the fragmented masses of the target and the projectile, respectively.

In the case of explosions, instead, the input data are the mass of the parent and a scale factor that has a unitary value for upper stages with a mass between 600 kg and 1000 kg.

The cumulative distribution of the number of fragments with respect to the characteristic length L_c, is estimated using Equation (4) for collisions and Equation (5) for explosions.

$$N = 0.1 \left(\frac{m_{frag}[\text{kg}]}{1[\text{kg}]} \right)^{0.75} \left(\frac{L_c[\text{m}]}{1[\text{m}]} \right)^{-1.71} \tag{4}$$

$$N = 6\, s \left(\frac{L_c[\text{m}]}{1[\text{m}]} \right)^{-1.6} \tag{5}$$

where N is the number of fragments, m_{frag} is the fragmented mass, and s is the scale factor. Then, the distribution of the number of fragments with respect to the A/M, for each characteristic length interval, is computed. For each pair of L_c-A/M intervals, values of characteristic length and area/mass ratio are extracted and then assigned to each fragment. It is assumed that within each interval there is a uniform probability distribution. The value of the area (A) for each fragment is computed as a function of its length L_c, using the following equation, valid both for collisions and explosions.

$$A = 0.556945 \, L_c^{2.0047077} \tag{6}$$

The mass value M of each fragment can then be estimated as follows.

$$M = A \left(\frac{M}{A} \right) \tag{7}$$

Finally, the distribution of the speed variations (ΔV) due to the event is computed and a ΔV value is assigned to each fragment by random extraction.

3. Breakup Model Sensitivity Analysis and Tuning Approach

The input data of the collision model are the masses of the parents and the impact velocity. The impact velocity (v_{imp}), normally computed from the state vectors of the parents, generally affects the fragmented mass during a collision. However, considering that the typical uncertainty in the knowledge of the impact velocity is in the order of m/s [34], this effect is very limited. Moreover, as long as the number of catalogued fragments is known, the impact velocity does not influence the iterative estimation of the fragmented mass but its computational cost. In fact, v_{imp} is used only for the computation of the specific kinetic energy and, hence, for the definition of the type of collision (i.e., catastrophic or non-catastrophic). Such definition determines the initial values with which the iterative algorithm starts. Therefore, the impact velocity does not affect the final value of the estimated fragmented masses but only the number of iterations needed to reach convergence. In particular, if the collision is catastrophic, the impact velocity has no effect on the number of iterations, since the initial value of the iterative approach would always be equal to the total mass of the parents, regardless of the value of v_{imp}. In case of a non-catastrophic collision, the impact velocity instead enters directly in Equations (2) and (3) to compute the estimated fragmented mass according to the SBM. This could lead to an increase of number of iterations, e.g., from 2 to 5. Based on these considerations, the masses of the parents are the only parameters to tune the model. The tuning of the masses can be done based on the accurate information provided by the catalogued fragments: namely, their number and orbital parameters. The orbital parameters available for the catalogued fragments can provide useful information on the ΔV distribution. However, such distribution seems to be rather insensitive to the input masses. To support this statement, a sensitivity analysis was carried out. For a fixed value of the projectile mass, set equal to 100 kg, the SBM was run for three different values of the target mass M_{targ} (i.e., 100 kg, 500 kg and 1000 kg), and three different values of the impact velocity v_{imp} (i.e., 1 km/s, 5 km/s and 10 km/s). For each couple (M_{targ}, v_{imp}), 100 runs were executed. For each run the mean μ and the standard deviation σ of the ΔV distribution were computed for all the fragments generated by the breakup (hereinafter called *population*) and for the fragments with a characteristic length greater than 10 cm (hereinafter called *sample*). Therefore, for each couple (M_{targ}, v_{imp}), a set of 100 means ($\mu_{\Delta V}$) and standard deviations ($\sigma_{\Delta V}$) is obtained. Figures 1–3 show the boxplots of $\mu_{\Delta V}$ and $\sigma_{\Delta V}$ in the different cases for the sample fragments. On each box, the central mark (i.e., the red line) indicates the median of the statistics parameter (i.e., $\mu_{\Delta V}$ and $\sigma_{\Delta V}$), the bottom and top edges of the box indicate the 25th and 75th percentiles, respectively. The difference between the 75th and 25th percentiles (i.e., the height of the box) is called interquartile range (IQR). The whiskers extend to a value equal to 1.5*IQR above the 75th percentile and 1.5*IQR below the 25th percentile. Outliers are the values

beyond the whiskers and are plotted individually using the '+' symbol. By looking at the mean and standard deviation distributions, for a fixed impact velocity, the ΔV distributions are statistically similar regardless of the target mass. In fact, applying a two-sample t-test to the ΔV distributions obtained with the same impact velocity and different target mass, the null hypothesis (i.e., the sample data are from populations whose expected means are the same) is accepted with 95% of confidence in all the cases. Moreover, the percentage variation of the median of the $\mu_{\Delta V}$ and $\sigma_{\Delta V}$ distributions was computed for target mass equal to 500 kg and 1000 kg with respect to the case in which the target mass is equal to 100 kg. The results of this analysis are reported in Table 1 considering different values of the impact velocity. The percentage variation is less than 5% for the median of $\mu_{\Delta V}$ and less than 10% for the median of $\sigma_{\Delta V}$.
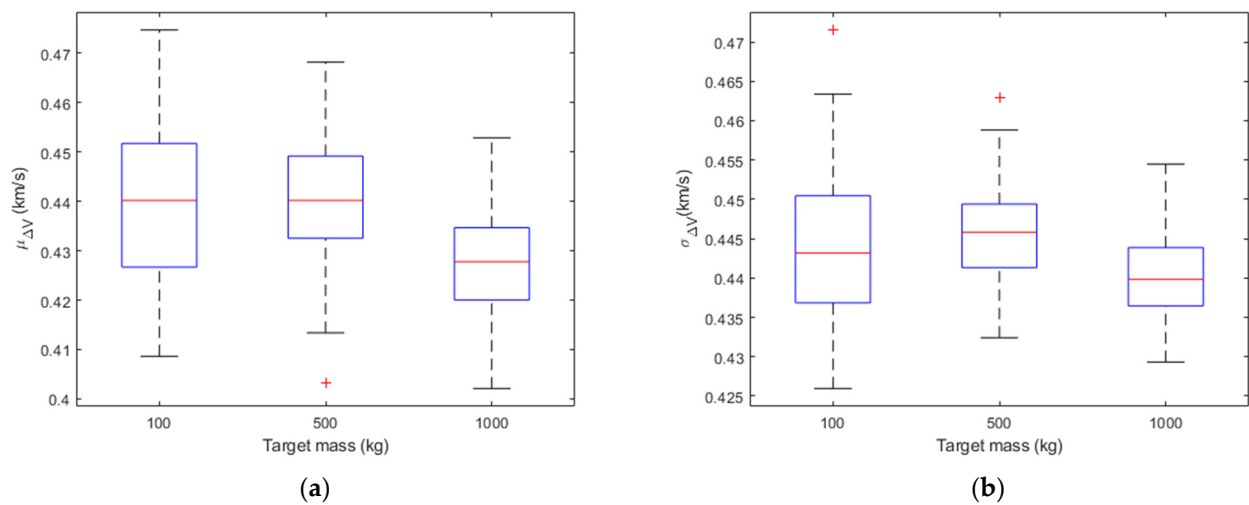

Figure 1. Mean (**a**) and standard deviation (**b**) of velocity distribution of sample fragments for different values of target mass for an impact velocity of 1 km/s. Mass of projectile is assumed to be 100 kg.
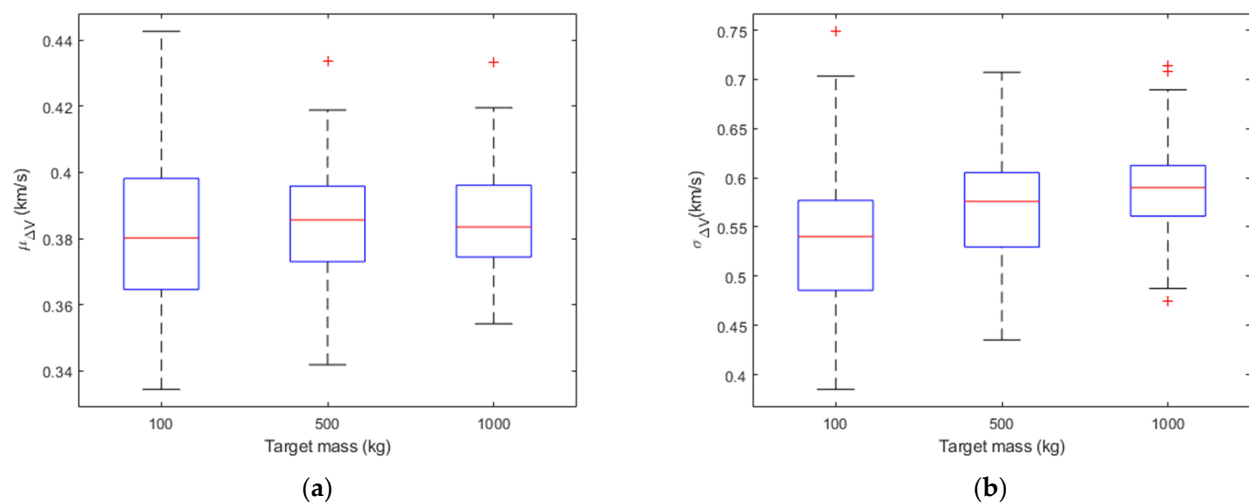

Figure 2. Mean (**a**) and standard deviation (**b**) of velocity distribution of sample fragments for different values of target mass for an impact velocity of 5 km/s. Mass of projectile is assumed to be 100 kg.
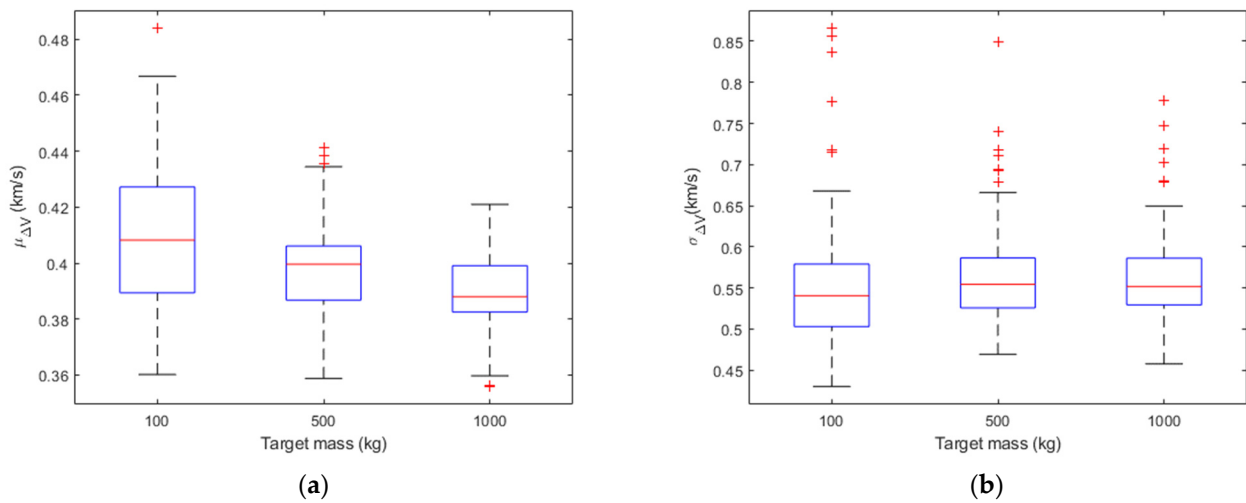
Figure 3. Mean (**a**) and standard deviation (**b**) of velocity distribution of sample fragments for different values of target mass for an impact velocity of 10 km/s. Mass of projectile is assumed to be 100 kg.

Table 1. Absolute percentage variation of $\mu_{\Delta V}$ and $\sigma_{\Delta V}$ distributions for target mass equal to 500 kg and 1000 kg with respect to target mass equal to 100 kg.

v_{imp} \ M_p	Absolute Percentage Variation of $\mu_{\Delta V}$ (%)		Absolute Percentage Variation of $\sigma_{\Delta V}$ (%)	
	500 kg	**1000 kg**	**500 kg**	**1000 kg**
1 km/s	0.3×10^{-2}	2.8	0.6	0.7
5 km/s	1.4	0.9	6.6	9.2
10 km/s	2.1	4.9	2.5	2.0

To further support the above statement, Figure 4 plots the median of the means of ΔV distributions against the impact velocity for the different values of the target mass. There is not a clear trend between the median of the mean of ΔV and the parent's mass. This analysis shows that, for a known impact velocity, the velocity distribution of the fragments is not significantly affected by the parent masses, and thus, cannot be used to estimate the fragmented mass.

Therefore, as in previous works [4,28] the parameters estimation is based on the number of catalogued objects. This approach, however, presents three main challenges. Firstly, the limitations of ground sensors introduce an observability gap. In fact, depending on the altitude, only fragments greater than a certain threshold, L_{min}, can be detected and tracked (e.g., L_{min} of order of 10 cm size at LEO and 1 m at GEO). Secondly, after a short time from the fragmentation event (FEV), the cloud of debris is not dispersed enough, and it is hard to correctly catalogue the different fragments of the cloud. Thirdly, especially for high energy collisions or for breakup events at lower orbits, a significant number of fragments decay due to the atmospheric drag. Thus, the epoch at which the fragments TLEs are known is important.
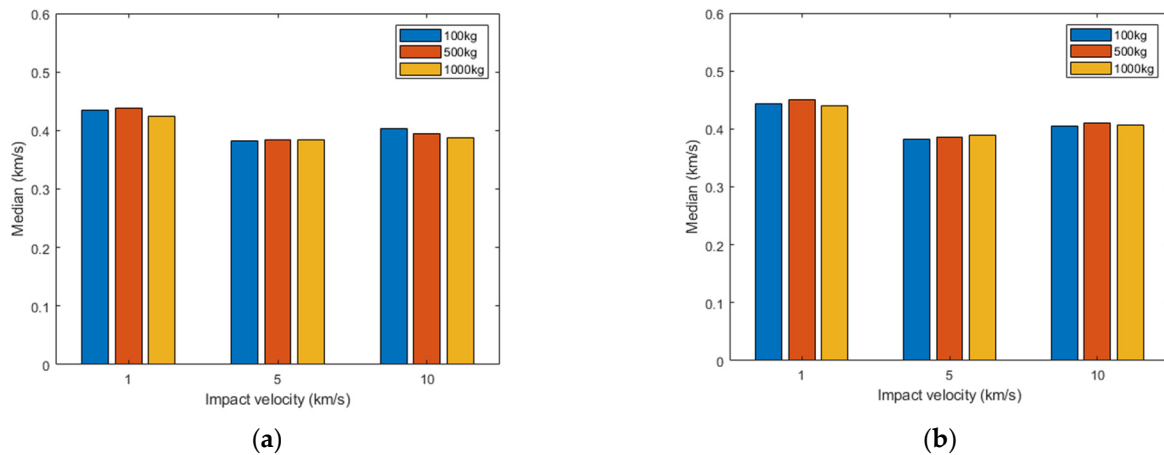
Figure 4. Median of target (**a**) and projectile (**b**) fragments sample velocities for different values of impact velocity and target mass. Mass of projectile is assumed to be 100 kg.

To better understand how to tune the model and to support the criteria adopted to filter the fragments generated by the SBM, a brief description of how the breakup model is implemented is provided. A scheme of the overall architecture is reported in Figure 5.

The developed model takes as inputs:

1. The type of input file to load (i.e., ephemerides or TLEs). In both cases, the software extracts the state vector of the parent(s), x, either directly, in the case of ephemerides, or converting the orbital parameters to position and velocity, in case of TLEs. Moreover, the impact velocity is computed as the norm of the relative velocity difference between the two colliding objects.

2. Mass and size of the parents

After the kinetic energy estimation and the classification of the type of collision, the distributions of the fragments' characteristics are estimated, as described in the previous section. Such distributions can be limited within user-defined intervals based on literature [12]. In particular, at each step of the area/mass extraction (and hence of each fragment mass assignment), a check on the mass conservation principle is carried out. Specifically, fragments are extracted according to the normal procedure as described in Section 2 until the difference between the sum of their masses (M_{tot}) and the mass of the parent is lower than a tolerance threshold (i.e., 5%). If the extraction procedure leads to a value of M_{tot} greater than the mass of the parent by more than 5%, the fragments with minimum A/M probability in the current L_c bin are removed. Then the ΔV distribution is estimated. The SBM only provides the distribution of the ΔV module for the fragments generated by the breakup event. To analyze the fragments' evolution, a direction must be assigned to each ΔV. This task must be done assuring that the conservation of momentum is met. Hence, an icosahedral grid was created whose nodes correspond to directions in a three-dimensional space [26]. It is assumed that each node has the same probability to be associated to each fragment. The ΔV, multiplied by the direction cosines corresponding to each direction, gives the velocity components of each fragment. Each fragment is therefore characterized by length, mass, area, and area/mass ratio, position at the fragmentation event (FEV), coinciding with the position of the parents, speed at FEV, computed as the sum between the speed of the parent and the ΔV. The obtained set of fragments is then filtered by removing objects characterized by:

-   length smaller than a threshold value (L_{thr}) defined by the user,
-   negative semimajor axis (SMA_{thr}), corresponding to a hyperbolic orbit, not of interest for the analyses of this paper. In fact, the possibility to track these fragments vanishes in time and their number is usually lower than 2% of the fragments over the size threshold.

- altitude at perigee lower than 120 km (h_{thr}), corresponding to a fragment that will re-enter before being catalogued.

The previous filtering is applied after assuring the conservation of momentum is achieved.
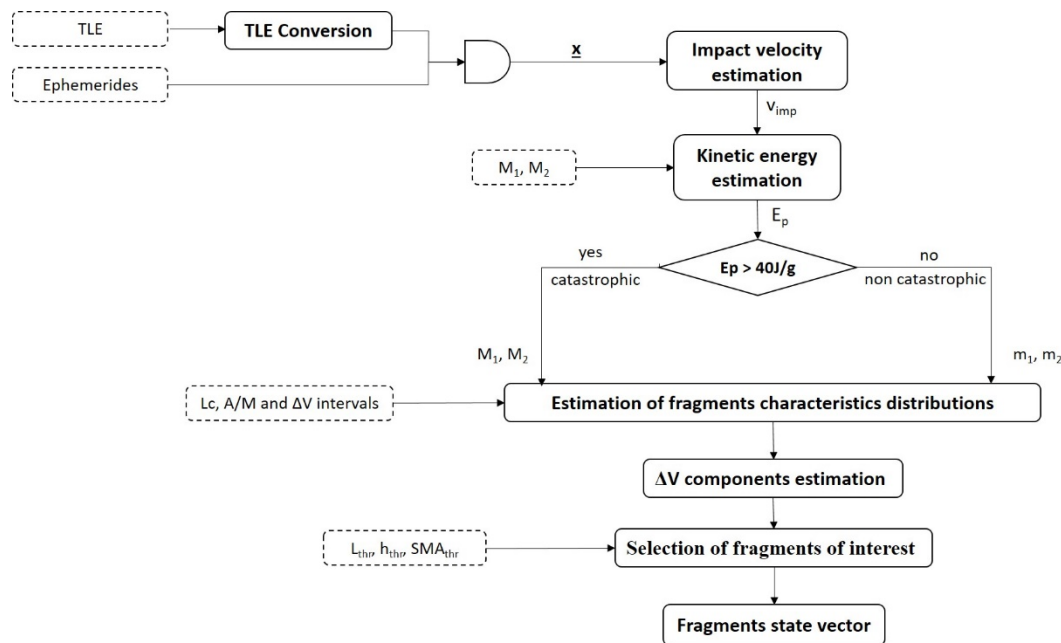

Figure 5. Scheme of SBM implementation. Each fragment is characterised by physical characteristics (i.e., size, mass, *A/M*) and a state vector (i.e., position and velocity).

The Iterative Approach

An iterative logic based on the TLEs of catalogued fragments relevant to a fragmentation event is adopted to determine the input parameters of the breakup model and obtain the same number of real fragments within a certain tolerance. For the scope of this work, it is assumed that at the altitude of interest, all the fragments greater than a predefined threshold were catalogued. The logic consists of five main steps (as illustrated in Figure 6):

1. The TLEs of the fragments are loaded and the orbital parameters are extracted. Let N_{cat} be the number of catalogued fragments.
2. A set of simulated fragments is generated from the breakup model using as default values the mass of the parents and their relative velocity. Let $N_{SBM,Lc}$ be the number of simulated fragments with a length greater than the predefined size threshold.
3. The catalogued fragments are backward propagated until the FEV. This helps to distinguish the two clusters of fragments belonging respectively to the target and the projectile out of a TLE file containing mixed fragments generated by the parents. The general principle is to compute the norm of the relative velocity between fragments and parents at FEV, and to assign each fragment to the parent corresponding to the minimum norm. In the case of orbital planes rotated by at least a few degrees with respect to each other, which will typically characterize collision geometries for very low eccentricity orbits, the concept has a direct analytical implementation based on inclinations and right ascension of the ascending node. In fact, it is well-known that a plane change requires a large value of the out-of-plane component of ΔV. This is confirmed also from historic breakups, registering a maximum plane change of 3 degrees for the fragments with respect to their parent's original orbit [22]. Therefore, it can be assumed that, even with high energy collisions, the breakup fragments will only be dispersed a small amount from the parents' orbital planes. Using the law of cosines for spherical triangles, the rotation of each fragment's orbital plane with respect to target and projectile ones is computed:

$$\theta_{targ} = \text{acos}\left(\cos\left(i_{frag}\right) \times \cos\left(i_{targ}\right) + \sin\left(i_{frag}\right) \times \sin\left(i_{targ}\right) \times \cos\left(\Omega_{targ} - \Omega_{frag}\right)\right) \quad (8)$$

$$\theta_{proj} = \text{acos}\left(\cos\left(i_{frag}\right) \times \cos\left(i_{proj}\right) + \sin\left(i_{frag}\right) \times \sin\left(i_{proj}\right) \times \cos\left(\Omega_{proj} - \Omega_{frag}\right)\right) \quad (9)$$

where: θ_{targ} and θ_{proj} are the angles between the fragment orbit plane and the orbit plane of target and projectile, respectively, i_{frag}, i_{targ}, and i_{proj} are the inclination of the fragment, target and projectile orbit planes, Ω_{frag}, Ω_{targ} and Ω_{proj} are the right ascension of the ascending node of the fragment, target and projectile orbit planes. If θ_{targ} is smaller (larger) than θ_{proj}, the fragment is assigned to the target (projectile).

This procedure allows splitting in two parts the iterative process and carrying out two separate analyses. Mass and cross section area of the fragments, necessary for the backward propagation, might be unknown, especially when a short time since the FEV passed. Therefore, a default value of *A/M* is assumed. However, the uncertainty on these values should not affect the out-of-plane dynamics and, hence, the assignment of the fragments to the two debris clouds.

4. Estimation of decayed fragments: due to a negative ΔV or to the atmospheric drag, some fragments may decay in the time frame, $\Delta t_{FEV,TLE}$, between the FEV epoch and the last available TLE epoch. The number of decayed fragments, N_{dec}, can be negligible in the iterative process when many catalogued fragments, N_{cat}, are available. However, when N_{cat} is small, the number of decayed objects might represent a significant percentage, thus affecting the estimation of the fragmented mass. To consider this aspect in the iterative process, N_{dec} must be estimated. This is done by counting all the $N_{SBM,Lc}$ fragments having an altitude at perigee below 150 km. It is indeed reasonable to consider that the fragments with this characteristic decayed in the time frame $\Delta_{FEV,TLE}$.

5. Iterative algorithm: the iterative algorithm operates until the following relationship is satisfied.

$$N_{cat} - tol \leq N_{Lc,nodec} \leq N_{cat} + tol \quad (10)$$

where *tol* is a tolerance margin, $N_{Lc,nodec}$ is the number of not decayed fragments larger than the threshold (i.e., $N_{SBM,Lc} - N_{dec}$). The values for the tolerances depend on the statistical variability of EVOLVE over different runs, which increases as the fragmented mass (and consequently, the number of catalogued fragments) reduces. So, for N_{cat} less than 50, a minimum tolerance of 0.3 N_{cat} is set. For N_{cat} in the range 50–100 and N_{cat} greater than or equal to 100, the tolerance values were scaled down (i.e., 0.2 N_{cat} and 0.1 N_{cat}, respectively). Figure 6 shows a scheme of the iterative logic implemented.

When Equation (10) is not satisfied, the bisection method is applied to estimate the tuning parameters. As stated in the previous section, the tuning parameters are the fragmented masses of the two parents. The bisection method is applied to the number of target and projectile fragments separately.
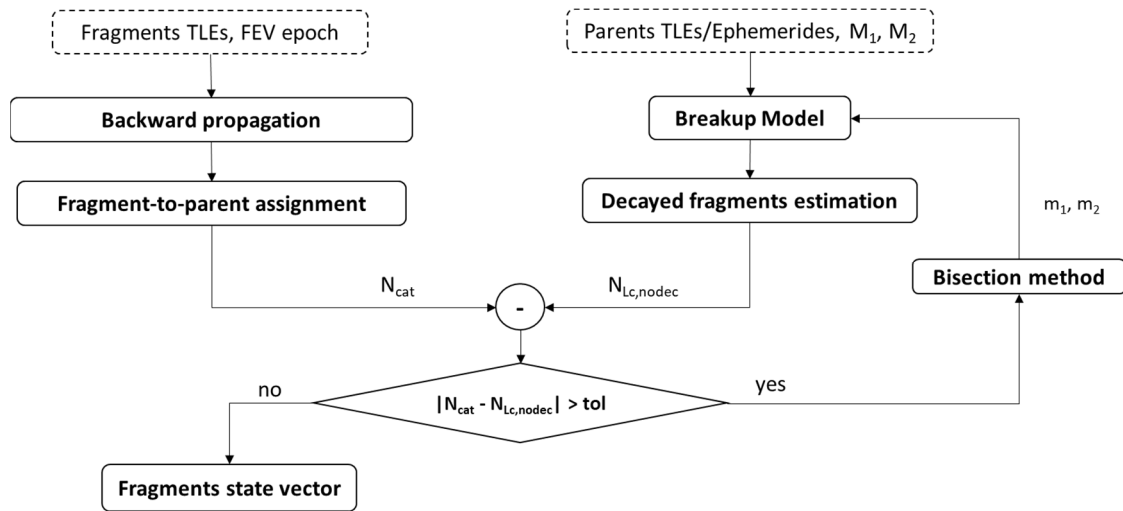
Figure 6. Scheme of iterative logic.

The inputs to the algorithm are the number of catalogued fragments from the target and projectile clouds ($N_{cat,targ}$ and $N_{cat,proj}$), the number of simulated fragments previously generated, with altitude of perigee greater than 150 km at FEV ($N_{Lc,nodec}$) and the mass $M_{SBM,i}$, with $i = 1,2$ (1 for the target and 2 for the projectile). $M_{SBM,i}$, is equal to the total parent mass (for catastrophic event) or the estimated fragmented mass by the SBM, according to Equations (2) and (3). If the number of simulated fragments is equal (within a certain percentage) to the number of real fragments, the algorithm is not executed, and the number of simulated fragments is the one generated by the SBM. Otherwise, the algorithm is executed. Let M_i be the initial mass of the i-th parent (i.e., $i = 1$ for the target and $i = 2$ for the projectile); $m_{i,j}$ be the estimated fragmented mass for the i-th parent at the j-th iteration; $m_{i,0} = M_{SBM,i}$, be the initial mass the bisection method starts with; $[a_j \ b_j]$ be the interval in which the bisection method is applied. For $j = 1$:

$$a_j = 0, \ b_j = M_i \tag{11}$$

then, if $N_{Lc,nodec} > N_{cat} + tol$:

$$m_{i,j} = \frac{m_{i,0}}{2} \tag{12}$$

both for catastrophic and non-catastrophic collision, while if $N_{Lc,nodec} < N_{cat} - tol$:

$$m_{i,j} = M_i \tag{13}$$

for catastrophic collision, and:

$$m_{i,j} = \frac{m_{i,0} + b_j}{2} \tag{14}$$

for non-catastrophic collision. For $j \geq 2$, both for catastrophic and non-catastrophic collisions:

$$m_{i,j} = \frac{a_j + b_j}{2} \tag{15}$$

where, if $N_{Lc,nodec} > N_{cat} + tol$:

$$[a_j \ b_j] = [a_{j-1} \ m_{i,j-1}] \tag{16}$$

while, if $N_{Lc,nodec} < N_{cat} - tol$:

$$[a_j \ b_j] = [m_{i, \ j-1} \ b_{j-1}] \tag{17}$$

Equations (15)–(17) are valid both for catastrophic and non-catastrophic collisions. In all the previous cases, the bisection method is lower bounded by zero mass and upper bounded by the initial parent's mass.

4. Results and Discussions

To demonstrate the effectiveness of the proposed iterative approach, two simulated and one real collision events are considered as test cases.

4.1. Simulated Collision Events

A collision is hypothesized assuming the masses of the parent objects, i.e., M_1 and M_2, the impact velocity and the corresponding fragmented masses (i.e., m_1 and m_2). By running the SBM using m_1 and m_2 as input masses, the reference values for the number of generated fragments, i.e., N_1 and N_2, can be obtained.

The goal of the proposed iterative approach is to estimate m_1 and m_2 assuming that all the observable fragments, i.e., those with characteristic length larger than 10 cm, are catalogued. To this aim, the iterative approach is applied using the total masses of the parents, i.e., M_1 and M_2, as initial guess. The SBM is then iterated until the convergence condition given by Equation (10) is met. At convergence, the number of generated fragments is indicated by $N_{1,est}$ and $N_{2,est}$, respectively, while the corresponding fragmented masses is indicated by $m_{1,est}$ and $m_{2,est}$, respectively.

The first test case is the simulation of a catastrophic collision. The orbital parameters of the simulated parents are listed in Table 2.

Table 2. Orbit parameters of parents.

Target					
a = 7359 km	e = 0.00348	i = 83°	Ω = 8.63°	ω = 237°	ν = 100°
Projectile					
a = 7461 km	e = 0.01459	i = 100°	Ω = 199.8°	ω = 240°	ν = 25°

With a, e, i, Ω, ω, ν being respectively the semimajor axis, eccentricity, inclination, right ascension of the ascending node, argument of perigee, and true anomaly.

The parent masses are M_1 = 1000 kg, M_2 = 800 kg and the impact velocity is equal to 14 km/s. It is assumed that only the following masses are involved in the fragment generation: m_1 = 850 kg, m_2 = 490 kg. With these values of masses, the SBM generates a set of N_1 = 693 fragments from the target and N_2 = 453 from the projectile.

The input data for the fragmented mass are set equal to the actual parent masses, i.e., M_1 = 1000 kg, M_2 = 800 kg, while v_{imp} is set to 14 km/s. The application of the standard SBM would produce a number of fragments, N_{SBM}, about 14% and 58% more than N_1 and N_2, respectively. However, after 3 iterations, the proposed approach reduces this overestimate to 0.9% and 2.2%, respectively, while allowing the estimation of the fragmented masses with an error with respect to the assumed values of about 3% and 2%, respectively. Simulation results are summarized in Table 3.

Table 3. Comparison between standard-SBM and iterative-SBM for first test case.

	Parents Mass	Assumed Fragmented Mass	N_{cat}	m_{est}	N_{est}	N_{SBM}
Target	1000 kg	850 kg	693	875 kg	699	793
Projectile	800 kg	490 kg	453	500 kg	463	716

Figure 7 shows the distribution of the reference fragments in the $i\sin(\Omega)$-$i\cos(\Omega)$ plane. In this plane, the distance of any point from the origin is equal to the inclination of the orbit plane of the fragment, while the ratio between the x-coordinate and the y-

coordinate is equal to the tangent of the RAAN. The set of fragments derived from target and projectile gather in two regions have the same inclination of the parent objects, with a certain dispersion due to the collision. This is further supported by Figure 8, representing the histograms of the reference and estimated fragments in the range 75–105 degrees of inclination. Figure 9 represents the histograms of the reference and estimated fragments in the range 6900–12,000 km of semi-major axis. This is representative of the ΔV distribution and shows how they are qualitatively similar in the two cases. This is further supported by the Gabbard diagrams in Figures 10 and 11.
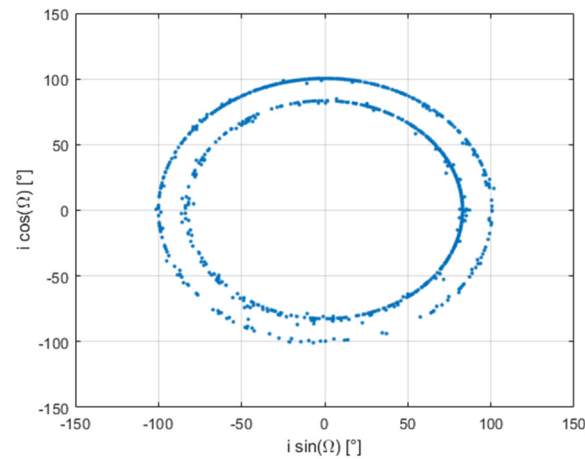
Figure 7. Distribution of reference fragments in plane $i\sin(\Omega)$-$i\cos(\Omega)$ for first test case.
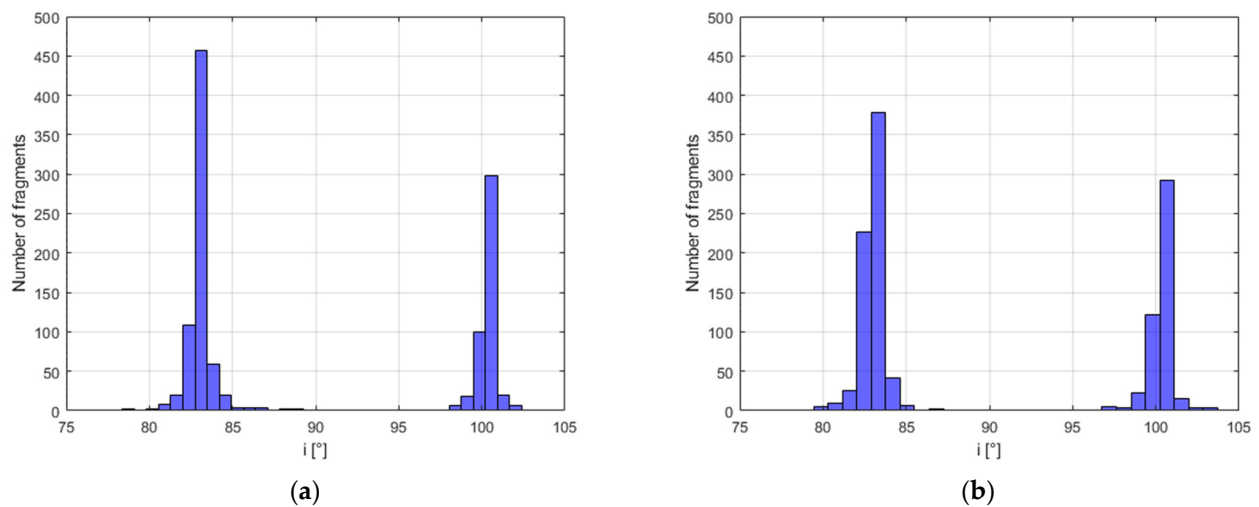

(**a**)   (**b**)

Figure 8. Histograms of reference (**a**) and estimated (**b**) fragments in range [75°, 105°] of inclination for first test case.
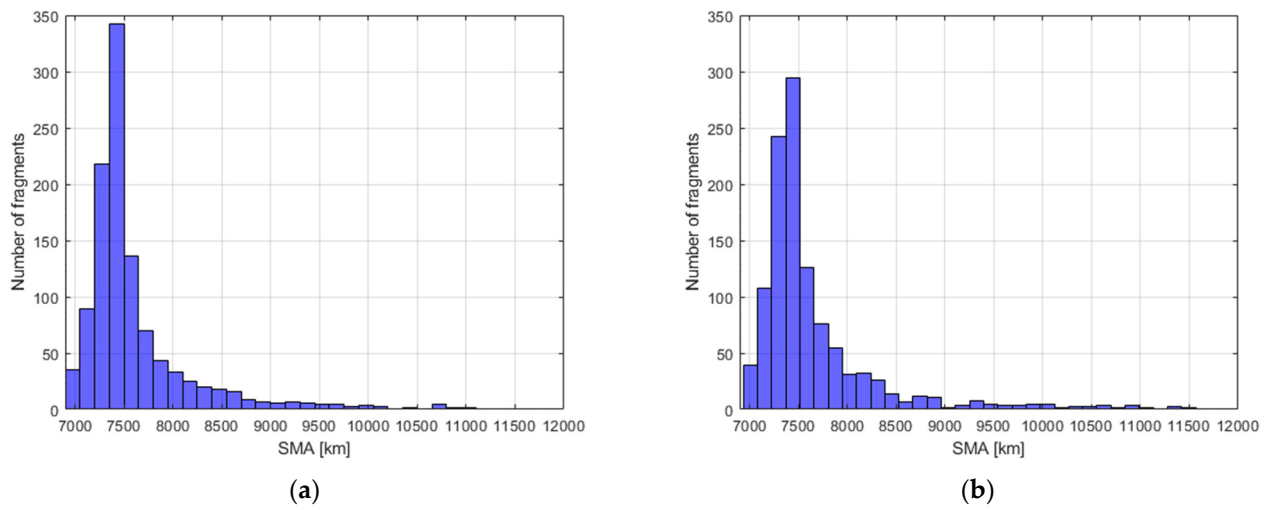
Figure 9. Histograms of reference (**a**) and estimated (**b**) fragments in range [6900, 12,000] km of semimajor axis for first test case.
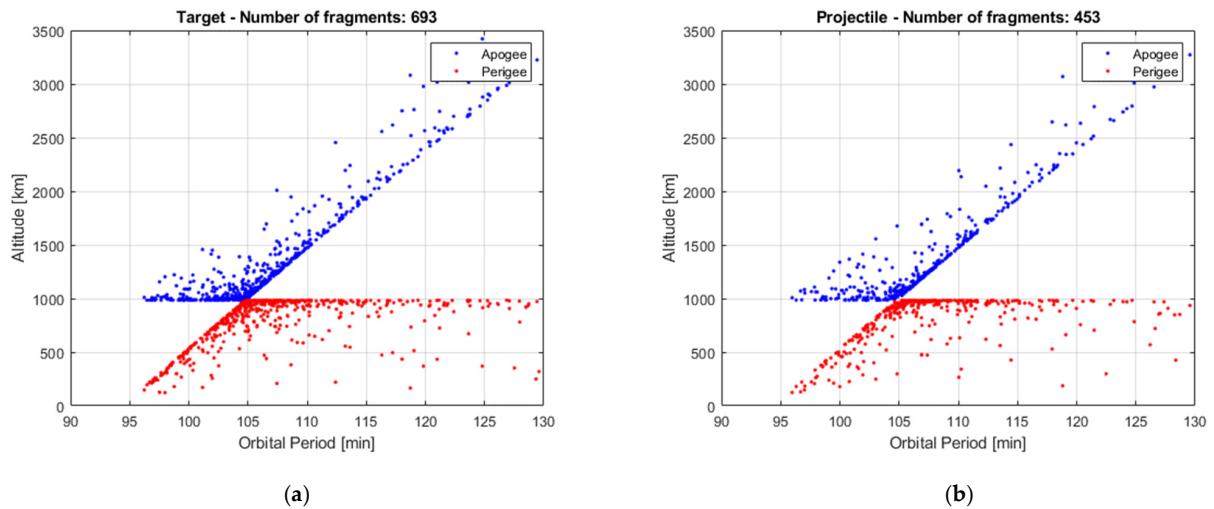

Figure 10. Gabbard diagrams for the target (**a**) and the projectile (**b**), obtained with input masses equal to $m_1 = 850$ kg and $m_2 = 490$ kg.
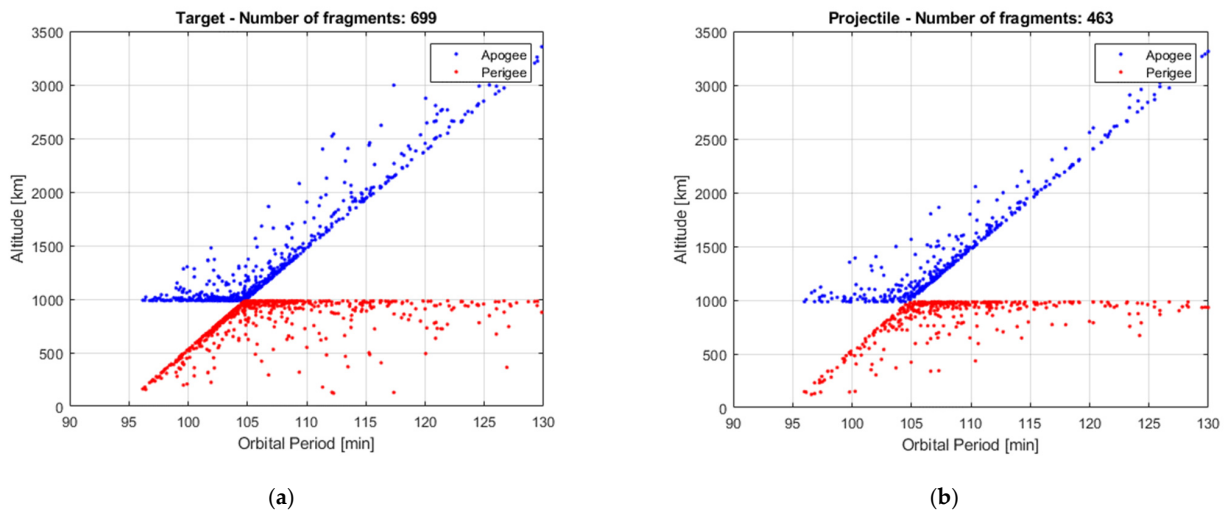

Figure 11. Gabbard diagrams for the target (**a**) and the projectile (**b**), obtained with fragmented masses estimated by iterative approach for first test case.

As stated in Section 1, a correct parent identification is not always guaranteed, and identification issues could lead to erroneously assigned objects. To consider this issue, an analysis of the method performance under this circumstance is carried out. It is assumed that a certain percentage of the projectile fragments was erroneously assigned to the target. In particular, the following percentages were considered: 2%, 4%, 10%, 15%, 20%. Table 4 reports the number of fragments assigned to each parent considering the previous percentages. The obtained number of fragments is rounded up.

Table 4. Values of N_{cat} for different percentages of assignment error.

Percentage Assignment Error	0%	2%	4%	10%	15%	20%
Target	693	703	712	739	761	784
Projectile	453	443	434	407	385	362

For each percentage assignment error, 100 runs were executed. For each run the mean μ_{nf} and the standard deviation σ_{nf} of the number of fragments greater than 10 cm, as well as the mean μ_{mf} and the standard deviation σ_{mf} of the estimated fragmented mass, were computed. Figure 12a shows the percentage error associated to μ_{nf} (solid line), $\mu_{nf} - \sigma_{nf}$ and $\mu_{nf} + \sigma_{nf}$ (error bars) for the target (in black) and the projectile (in red). Similarly, Figure 12b shows the percentage error associated to μ_{mf} (solid line), $\mu_{mf} - \sigma_{mf}$ and $\mu_{mf} + \sigma_{mf}$ (error bars) for the target (in black) and the projectile (in red). It must be pointed out that, for assignment errors lower than 10%, the output error is not necessarily due to the erroneous number of catalogued fragments, but also depends on the statistical variability of EVOLVE.
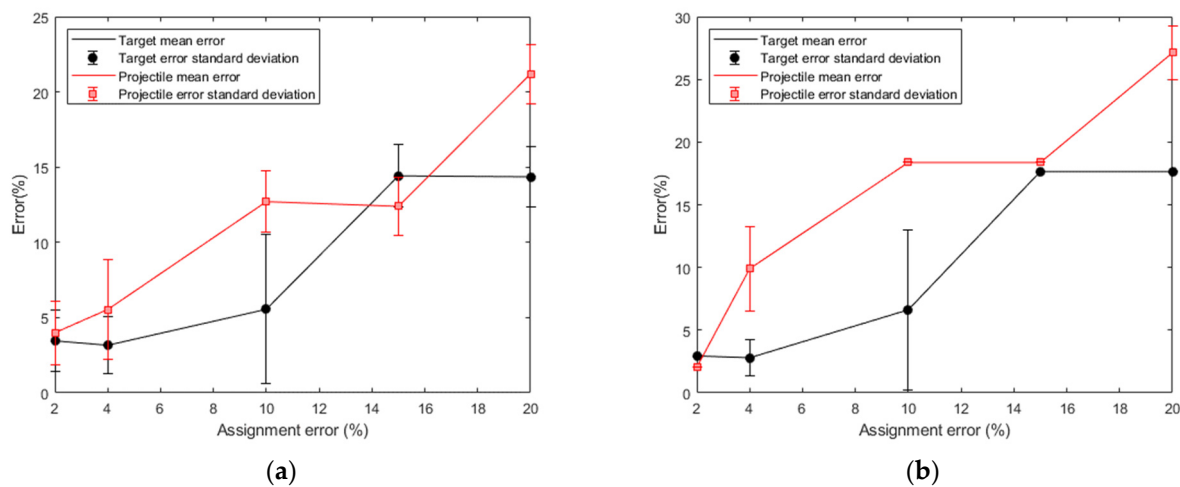

(a)   (b)

Figure 12. (**a**) Mean and standard deviation errors for number of fragments greater than 10 cm, both for target and projectile. (**b**) Mean and standard deviation errors for estimated fragmented mass, both for target and projectile.

The second test case regards a non-catastrophic collision. The orbital parameters of the simulated parents are listed in Table 5.

Table 5. Orbit parameters of parents.

Target					
$a = 7361$ km	$e = 8.9 \times 10^{-5}$	$i = 90°$	$\Omega = 45°$	$\omega = 90°$	$\nu = 0°$
Projectile					
$a = 7361$ km	$e = 8.9 \times 10^{-5}$	$i = 90°$	$\Omega = 53°$	$\omega = 90°$	$\nu = 0°$

The parent masses are M_1 = 1000 kg, M_2 = 50 kg, and the impact velocity is equal to 1 km/s. It is assumed that only the following masses are involved in the collision: m_1 = 30 kg, m_2 = 30 kg. With these values of masses, the SBM generates a set of N_1 = 37 fragments from the target and N_2 = 38 from the projectile (as illustrated in Table 6), considered as reference values. The input data are then set equal to the actual parent masses, i.e., M_1 = 1000 kg, M_2 = 50 kg while v_{imp} is still equal to 1 km/s. Without the iterative approach, the SBM estimates fragmented masses, M_{SBM}, of 50 kg for both the target and the projectile (about 67% more than the assumed involved mass), while the number of generated fragments is equal to 68 and 74. Instead, the iterative approach allows reducing the fragmented mass estimation error down to about 17% of the assumed values. With regards to the number of fragments the SBM commits an error of 84% for the target and 94% for the projectile, while these values are reduced to about 8% and 13% by applying the iterative approach. These results are in accordance with Pardini and Anselmo [27] that highlight how the outputs of the non-catastrophic collisions are worse than catastrophic collisions in the estimation of the number of fragments. The output of the second test case is summarized in Table 6.

Table 6. Comparison between standard-SBM and iterative-SBM for second test case.

	Parents Mass	Assumed Fragmented Mass	N_{cat}	M_{SBM}	m_{est}	N_{SBM}	N_{est}
Target	1000 kg	30 kg	37	50 kg	25 kg	68	34
Projectile	50 kg	30 kg	38	50 kg	25 kg	74	33

Figure 13 shows the distribution of the reference fragments in the $i\sin(\Omega)$-$i\cos(\Omega)$ plane. Differently from the first test case, the set of fragments derived from target and projectile lie on the same circle corresponding to an inclination of 90 degrees. This is further supported by Figure 14, representing the histograms of the reference and estimated fragments in the range [80, 100] degrees of inclination. Figure 15 represents the histograms of the reference and estimated fragments in the range [6900, 12,000] km of semimajor axis. This is representative of the ΔV distribution and show how they are qualitatively similar in the two cases. The Gabbard diagrams in Figures 16 and 17 further support this statement.
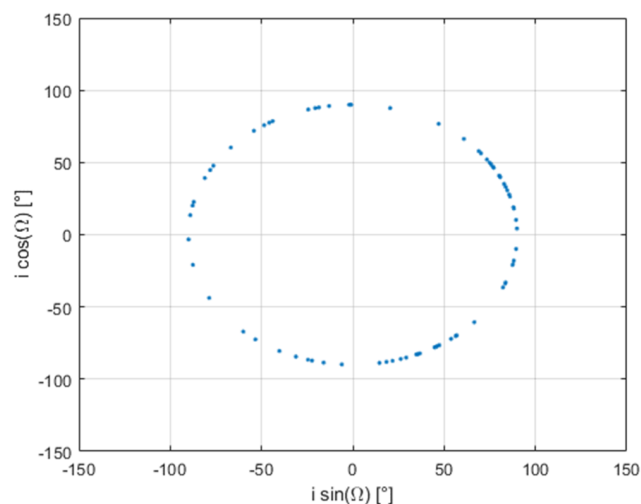

Figure 13. Distribution of reference fragments in plane $i\sin(\Omega)$-$i\cos(\Omega)$ for second test case.
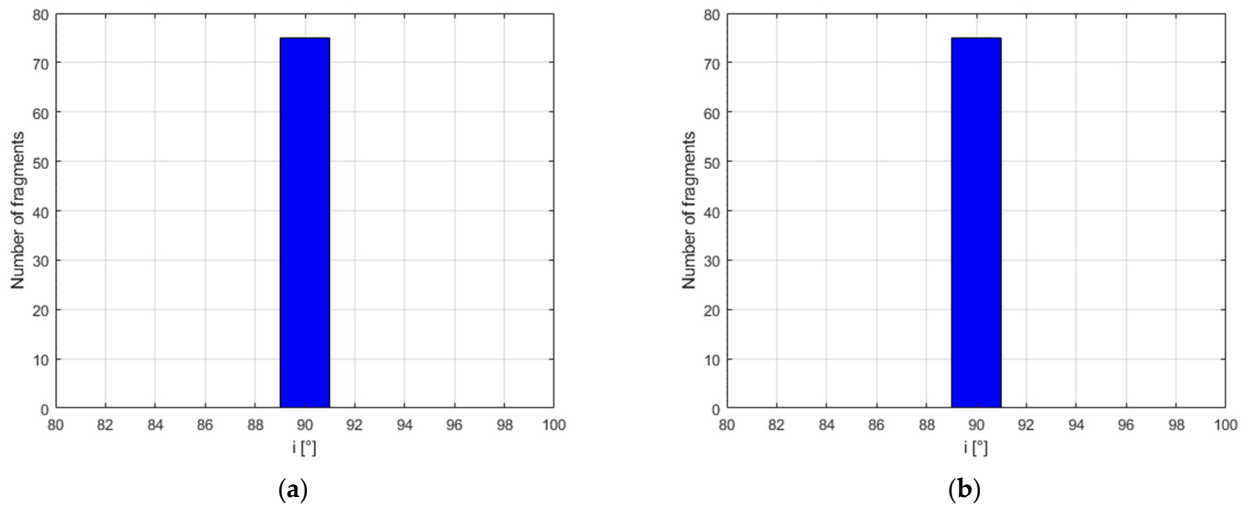
Figure 14. Histograms of reference (**a**) and estimated (**b**) fragments in range [80°, 100°] of inclination for second test case.
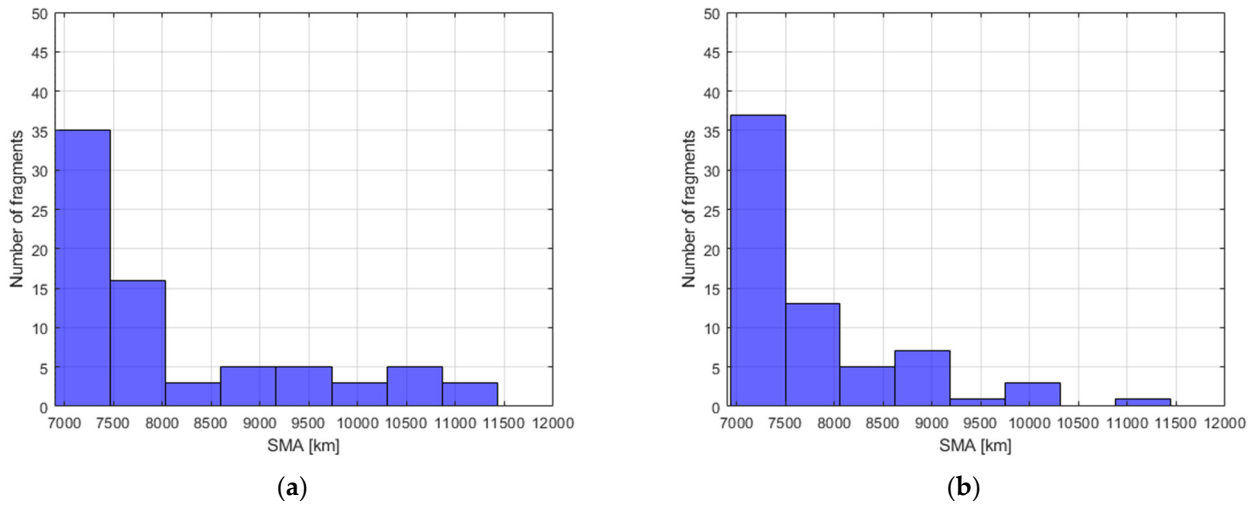

Figure 15. Histograms of reference (**a**) and estimated (**b**) fragments in range [6900, 12,000] km of semimajor axis for second test case.
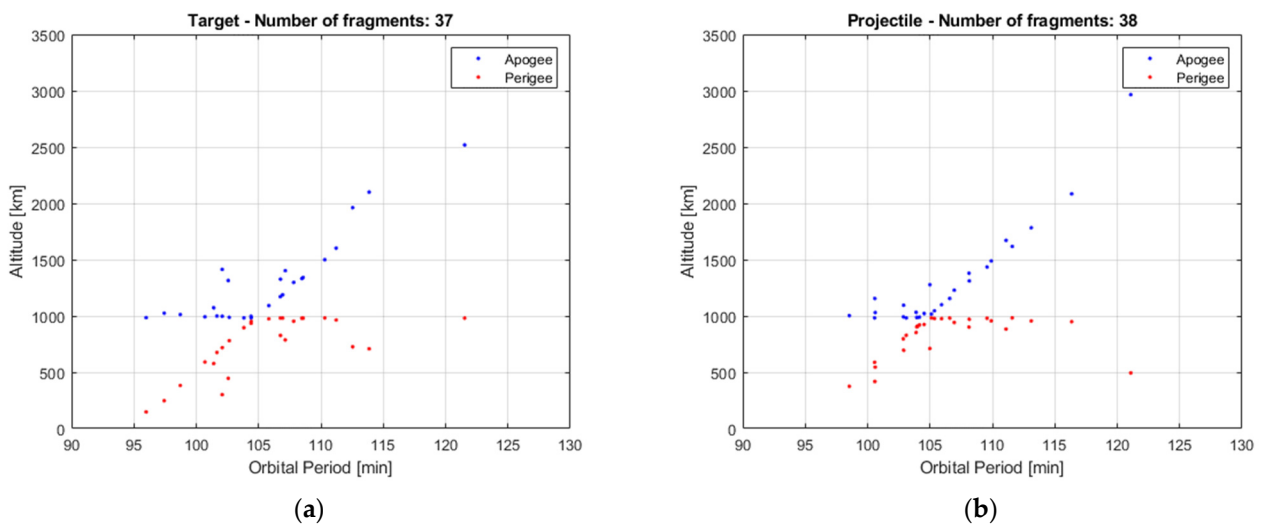

Figure 16. Gabbard diagrams for the target (**a**) and the projectile (**b**), obtained with input masses equal to m_1 = 30 kg and m_2 = 30 kg.
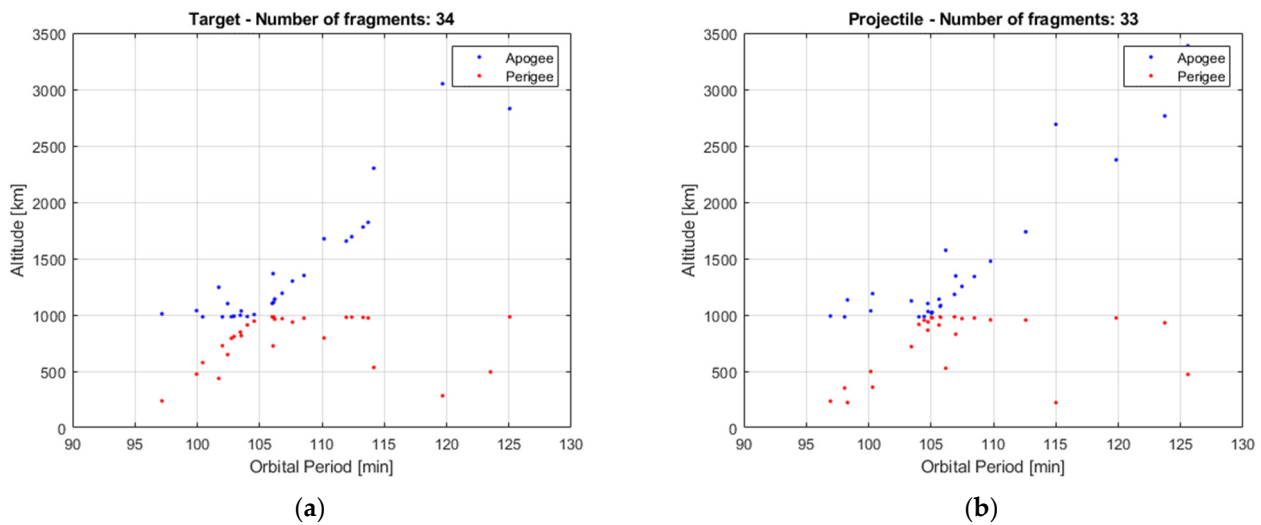
Figure 17. Gabbard diagrams for the target (**a**) and the projectile (**b**), obtained with fragmented masses estimated by iterative approach for second test case.

4.2. Real Collision Event

The third test case is a real fragmentation event, namely the on-orbit collision between DMSP 5B F5 Thor Burner 2A (i.e., target) and the Catalogued debris 26,207 (i.e., projectile) happened on 17 January 2005 [27]. Thor Burner 2A had a mass of 50 kg while the debris had a mass of 2.1 kg. The two objects collided at an altitude of 885 km with an impact velocity of 5.7 km/s. According to the SBM, since the energy-to-mass ratio is 62 J/g, the event is catastrophic and the number of fragments over 10 cm would be equal to 64 for the target and 0 for the projectile. However, only 6 fragments were catalogued [27]. Hence, the SBM overestimates the number of target fragments by 967%. Assuming that all the catalogued fragments are associated to the target, the iterative approach, instead, estimates a fragmented mass of 18.75 kg for the target and 2.1 kg (i.e., the total mass) for the projectile. The number of fragments generated are $N_{1_{frag}} = 6$ and $N_{2_{frag}} = 0$ in accordance with the catalogue. Table 7 summarizes all the data.

Table 7. Comparison between standard-SBM and iterative-SBM for real test case.

	Parents Mass	M_{SBM}	m_{est}	N_{SBM}	N_{est}
Target	50 kg	50 kg	18.75 kg	64	6
Projectile	2.1 kg	2.1 kg	2.1 kg	0	0

In all the previous test cases, the iterative approach provided reasonable tuning parameters to have a number of estimated fragments within a certain predefined interval. It is important to highlight that, even if theoretically possible, it is not useful to further reduce the percentage error. Indeed, due to the statistical nature of the SBM and the random extraction of the fragments' characteristics, the output could have a variance greater than the pre-defined percentage error.

Some further considerations can be made with respect to the number of fragments. When the number of catalogued fragments is relatively large (e.g., more than 50 fragments), after breakup model tuning it is possible to extract from the simulated distributions sets of fragments which are consistent with the observed ones. When the number of catalogued fragments is very small, two major concerns arise. On the one hand, the type of fragmentation event (i.e., collision or explosion) may be itself uncertain. On the other hand, while it is possible to verify the consistency of observed data with theoretical distributions, the phenomenon cannot be replicated in simulations by random extractions.

4.3. Computational Cost Analysis

In general, the computational cost characterizing the proposed method is mostly related to the run of the SBM and so to the number of iterations required to reach convergence.

For the sake of analyzing the effect of the tolerance on the number of iterations, an additional simulated test case is considered. Two parents with mass equal to 800 kg collide with an impact velocity of 10 km/s. The collision is theoretically catastrophic. The algorithm is executed considering three different subcases: N_{cat} greater than 100 (i.e., 500), between 50 and 100 (i.e., 60), and below 50 (i.e., 20) for both the parents. Figure 18 shows the number of iterations required, for the target (solid line) and the projectile (dashed line), to reach the convergence versus a tolerance value on N_{cat} equal to 5%, 10%, 20% and 30%. In all cases, a relatively small number of iterations is required to reach convergence.
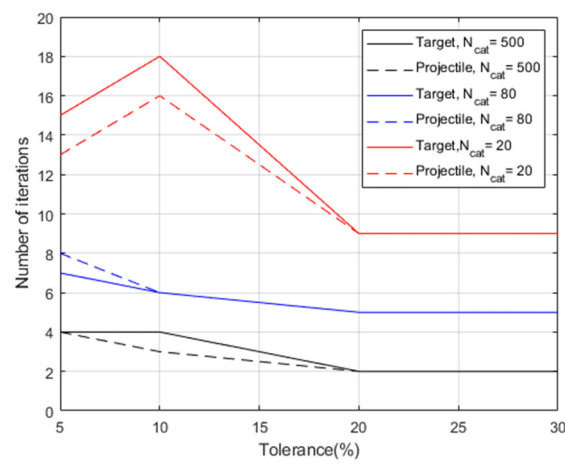

Figure 18. Number of iterations against tolerance on number of catalogued fragments for different values of N_{cat}, both for target (solid line) and projectile (dashed line).

5. Conclusions

This paper proposed an iterative approach to estimate the tuning parameters for the Standard Breakup Model, i.e., the fragmented mass of the parent objects in case of collision events. A sensitivity analysis was performed and demonstrated that the parents' masses do not affect the velocity distribution of the fragments. Therefore, the tuning of the masses cannot be based on the orbital parameters of the fragments but rather on the number of catalogued objects. The catalogued objects are backward propagated to the fragmentation event epoch and separated into two clusters corresponding to the target and projectile debris clouds. This allows performing the iterative approach on the two parent objects separately and, hence, estimating their fragmented masses. The approach was applied to three test cases, namely two simulated collisions (one catastrophic, and one non-catastrophic), and a real fragmentation event (on-orbit collision between DMSP 5B F5 Thor Burner and the Catalogued debris 26207). In all the cases, the algorithm has converged and provided reasonable values of the tuning parameters, obtaining a number of fragments equal, within a certain tolerance, to the number of catalogued objects. In particular, for the non-catastrophic collision and the real fragmentation event, big discrepancies were detected between the fragmented mass and number of fragments estimated by the SBM with nominal parameters, and the same outputs obtained by the iterative approach, with the latter being much closer to expected and real data. This also means that the tuned SBM can be used to better assess the number and distributions of nondetectable fragments generated by the collision event.

Author Contributions: Conceptualization, N.C., G.I., R.O. and G.F.; methodology, N.C., G.I., R.O. and G.F.; resources, A.B., A.R., M.P., A.P. and A.C.; supervision, R.O. and G.F.; writing—original draft, N.C.; writing—review & editing, G.I., R.O., G.F., A.B., A.R., M.P., A.P. and A.C. All authors have read and agreed to the published version of the manuscript.

References

1. ESA Space Debris Office. ESA's Annual Space Environment Report. Issue 5.0, 27 May 2021. Available online: https://sdup.esoc.esa.int/discosweb/statistics/ (accessed on 9 July 2021).
2. Mehrholz, D.; Leushacke, L.; Flury, W.; Jehn, R.; Klinkrad, H.; Landgraf, M. Detecting, Tracking and Imaging Space Debris. *ESA Bull.* **2002**, *109*, 128–134.
3. Lewis, H.G. Understanding long-term orbital debris population dynamics. *J. Space Saf. Eng.* **2020**, *7*, 164–170. [CrossRef]
4. Braun, V.; Lemmens, S.; Reihs, B.; Krag, H.; Horstmann, A. Analysis of breakup events. In Proceedings of the 7th European Conference on Space Debris, ESOC, Darmstadt, Germany, 18–21 April 2017.
5. Rossi, A.; Anselmo, L.; Pardini, C.; Jehn, R.; Valsecchi, G.B. The new space debris mitigation (SDM 4.0) long term evolution code. In Proceedings of the 5th European Conference on Space Debris, ESOC, Darmstadt, Germany, 30 March–2 April 2009.
6. Johnson, N.L. Space Debris Modeling at NASA. In Proceedings of the 3rd European Conference on Space Debris, ESOC, Darmstadt, Germany, 19–21 March 2001.
7. Krisko, P.H. The New NASA Orbital Debris Engineering Model ORDEM 3.0. In Proceedings of the AIAA/AAS Astrodynamics Specialist Conference, San Diego, CA, USA, 4–7 August 2014. [CrossRef]
8. Krisko, P.H.; Hall, D.T. Geosynchronous region orbital debris modelling with GEO_EVOLVE 2.0. *Adv. Space Res.* **2004**, *34*, 1166–1170. [CrossRef]
9. Krisko, P.H.; Liou, J.-C. NASA long-term orbital debris modelling comparison: LEGEND and EVOLVE. In Proceedings of the 54th International Astronautical Congress of the International Astronautical Federation, the International Academy of Astronautics, and the International Institute of Space Law, Bremen, Germany, 29 September–3 October 2003. [CrossRef]
10. Liou, J.-C.; Johnson, N.L. Instability of the Present LEO Satellite Populations. *Adv. Space Res.* **2008**, *41*, 1377–1384. [CrossRef]
11. White, A.E.; Lewis, H.G. An Adaptive Strategy for Active Debris Removal. *Adv. Space Res.* **2014**, *53*, 1195–1206. [CrossRef]
12. Johnson, N.L.; Krisko, P.H.; Liou, J.-C.; Anz-Meador, P.D. NASA's new breakup model of EVOLVE 4.0. *Adv. Space Res.* **2001**, *28*, 1046–1053. [CrossRef]
13. Liou, J.-C.; Clark, S.; Fitz-Coy, N.; Huynh, T.; Opiela, J.; Polk, M.; Roebuck, B.; Rushing, R.; Sorge, M.; Werremeyer, M. DebriSat—A planned laboratory-based satellite impact experiment for breakup fragment characterization. In Proceedings of the 6th European Conference on Space Debris, ESOC, Darmstadt, Germany, 22–25 April 2013.
14. Fonder, G.; Hughes, M.; Dickson, M.; Schoenfeld, M.; Gardner, J. Space Fence Radar Overview. In Proceedings of the International Applied Computational Electromagnetics Society Symposium (ACES), Miami, FL, USA, 14–19 April 2019.
15. Griffith, N.; Lu, E.; Nicolls, M.; Park, I.; Rosner, C. Commercial Space Tracking Services for Small Satellites. In Proceedings of the 33rd Annual AIAA/USU Conference on Small Satellites, Logan, UT, USA, 3–8 August 2019.
16. Muntoni, G.; Montisci, G.; Pisanu, T.; Andronico, P.; Valente, G. Crowded Space: A Review on Radar Measurements for Space Debris Monitoring and Tracking. *Appl. Sci.* **2021**, *11*, 1364. [CrossRef]
17. Diserens, S.; Lewis, H.G.; Fliege, J. NewSpace and its implications for space debris models. *J. Space Saf. Eng.* **2020**, *7*, 502–509. [CrossRef]
18. Murray, J.; Cowardin, H.; Liou, J.-C.; Sorge, M.; Fitz-Coy, N.; Huynh, T. Analysis of the DebriSat Fragments and Comparison to the NASA Standard Satellite Breakup Model. In Proceedings of the 1st International Orbital Debris Conference, Sugar Land, TX, USA, 9–12 December 2019.
19. Rivero, M.; Kleespies, J.; Patankar, K.; Fitz-Coy, N.; Liou, J.-C.; Sorge, M.; Huynh, T.; Opiela, J.; Krisko, P.; Cowardin, H. Characterization of debris from DebriSat hypervelocity test. In Proceedings of the 66th International Astronautical Congress, Jerusalem, Israel, 12–16 October 2015.
20. Murakami, J.; Hanada, T.; Liou, J.-C.; Stansbery, E. Micro-satellite impact tests to investigate multi-layer insulation fragments. In *Orbital Debris Quarterly News*; Space Systems Dynamics Laboratory: Fukuoka, Japan, 2009; Volume 13.
21. Hanada, T.; Liou, J.-C.; Nakajima, T.; Stansbery, E. Outcome of recent satellite impact experiments. *Adv. Space Res.* **2009**, *44*, 558–567. [CrossRef]
22. Hoots, F.; Sorge, M. Satellite Breakup Parameter Determination. *J. Astronaut. Sci.* **2012**, *59*, 120–140. [CrossRef]
23. Mains, D.; Sorge, M. Integrated breakup modeling solutions from DebriSat analysis. *J. Space Saf. Eng.* **2020**, *7*, 230–234. [CrossRef]
24. Sorge, M. Satellite Fragmentation Modeling with IMPACT. In Proceedings of the AIAA/AAS Astrodynamics Specialist Conference and Exhibit, Honolulu, HI, USA, 18–21 August 2008. [CrossRef]
25. Anz-Meador, P.D.; Matney, M.J. An assessment of the NASA explosion fragmentation model to 1 mm characteristic sizes. *Adv. Space Res.* **2004**, *34*, 987–992. [CrossRef]
26. Vallado, D.A.; Oltrogge, D.L. Fragmentation event debris field evolution using 3D volumetric risk assessment. In Proceedings of the 7th European Conference on Space Debris, ESOC, Darmstadt, Germany, 18–21 April 2017.
27. Pardini, C.; Anselmo, L. Review of past on-orbit collisions among catalogued objects and examination of the catastrophic fragmentation concept. *Acta Astronaut.* **2014**, *100*, 30–39. [CrossRef]
28. Letizia, F. Space Debris Cloud Evolution in Low Earth Orbit. Ph.D. Thesis, University of Southampton, Southampton, UK, February 2016.

29. Frey, S.; Colombo, C.; Lemmens, S. Advancement of a density-based debris fragment model and application to on-orbit break-up localisation. In Proceedings of the 36th IADC Plenary Meeting, Tsukuba, Japan, 5–8 June 2018.

30. Frey, S.; Colombo, C.; Lemmens, S. Density based modelling and indication of break-up location and epoch from fragments using backwards propagation. In Proceedings of the 5th European Workshop on Space Debris Modelling and Remediation, Paris, France, 25–27 June 2018.

31. Tetreault, K.; Ross, S.D.; Schroeder, K.; Black, J. Fragmentation Event Identification Using Back Propagation with Variable Ballistic Coefficient Calculation. In Proceedings of the 19th annual Advanced Maui Optical and Space Surveillance Technologies Conference (AMOS), Maui, HI, USA, 11–14 September 2018.

32. Dimare, L.; Cicalò, S.; Rossi, A.; Alessi, E.M.; Valsecchi, G.B. In-orbit fragmentation characterization and parent bodies identification by means of orbital distances. In Proceedings of the 1st International Orbital Debris Conference (IOC), Sugarland, TX, USA, 9–12 December 2019.

33. Romano, M.; Muciaccia, A.; Trisolini, M.; Di Lizia, P.; Colombo, C.; Di Cecco, A.; Salotti, L. PUZZLE Software for the Characterization of In-Orbit Fragmentation. In Proceedings of the 8th European Conference on Space Debris (Virtual), Darmstadt, Germany, 20–23 April 2021.

34. Geul, J.; Mooij, E.; Noomen, R. TLE uncertainty estimation using robust weighted differencing. *Adv. Space Res.* **2017**, *59*, 2522–2535. [CrossRef]